Journal of Power Sources, 43–44 (1993) 487–492

All-solid-state lithium microbatteries

Xuejie Huang*, Liquan Chen** and Joop Schoonman
Delft University of Technology, Laboratory for Inorganic Chemistry, Julianalaan 136, 2628 BL Delft, (Netherlands)

Abstract

All-solid-state lithium microbatteries were fabricated using the ceramic superconductor $YBa_2Cu_3O_{7-\delta}$ as cathode, and a PAN-based polymer as electrolyte. The employed cathode films had a thickness of about 10 μm. The charge and discharge current can reach values up to 100 $\mu A/cm^2$ at room temperature. The performance of the microbatteries was evaluated by cyclic voltammetry and a.c. impedance spectroscopy measurements. The batteries exhibit a good cycle life, capacity and efficiency.

Introduction

Solid polymer electrolyte lithium batteries have been investigated for many years [1]. They combine the use of thin-film Li ion-conducting polymer electrolytes with Li ion reversible electrodes. Improvements in the electronics industry and the miniaturization of electronic devices have reduced the current and power requirements for some devices to extremely low levels. The volumetric energy density of a battery (W h/l) is sometimes more important than the gravimetric energy density (W h/kg), because the volume of a battery is limited.

$YBa_2Cu_3O_{7-\delta}$ has been investigated as cathode material [2]. It has a high electronic conductivity, an open layer structure, a high density and exhibits good Li^+ diffusion. PAN–EC–PC–$LiClO_4$ has a high Li ionic conductivity at room temperature and shows a very good mechanical strength [3, 4].

In this paper the properties of a composite film comprising a $YBa_2Cu_3O_{7-\delta}$ cathode film and a PAN-based electrolyte film will be presented.

Experimental

The preparation of the PAN–EC–PC–$LiClO_4$ has been described in detail in ref. 4. The starting material of $YBa_2Cu_3O_{7-\delta}$ was prepared by a convenient ceramic processing technique [5]. Ball milling was used to obtain the powder.

We prepared two kinds of cathode-electrolyte laminar structures: (A) 90 wt.% $YBa_2Cu_3O_{7-\delta}$ + 10 wt.% electrolyte covered with electrolyte, and (B) 95 wt.% $YBa_2Cu_3O_{7-\delta}$ + 5 wt.% carbon black covered with electrolyte.

*Author to whom correspondence should be addressed.
**Permanent address: Institute of Physics, Academia Sinica, P.O. Box 603, Beijing 100080, China.

0378-7753/93/$6.00

In the preparation, the electrode powder was dispersed in dimethyl formamide to form a paste. Using doctor blading, a smooth film of the cathode material on a stainless-steel current collector was made of this paste. The cathode film thickness was about 10 μm. Subsequently, a dilute solution of the PAN-based electrolyte in DMF was applied on the surface of the cathode film. The electrolyte film was formed during evaporation of the solvent. The laminar structure had a total thickness of about 20 μm.

In order to form the thin-film battery a Li foil with a thickness of about 10 μm, which was made by pressing a Li pellet between two stainless-steel plates, was pressed against the laminar structure. The Li foil was covered with a stainless-steel end plate. A schematic presentation of the microbattery configuration is given in Fig. 1.

The charge, discharge and cycling behaviour of the batteries were recorded using a PAR 273 potentiostat. The batteries were cycled between 1.8 and 3.6 V at 0.2 mV/s. About 60% of the total capacity was utilized in a charge/discharge cycle.

Impedance spectroscopy of the microbatteries was performed using a Solartron 1270 frequency response analyser and a Solartron 1286 electrochemical interface. The impedance spectra were analysed using a non-linear least-squares (NLLS) computer fit programme developed by Boukamp of the Faculty of Chemical Technology, University of Twente, the Netherlands. Impedance data were recorded at the equilibrium potential, i.e., under conditions of absence of d.c. current flow.

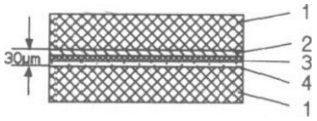

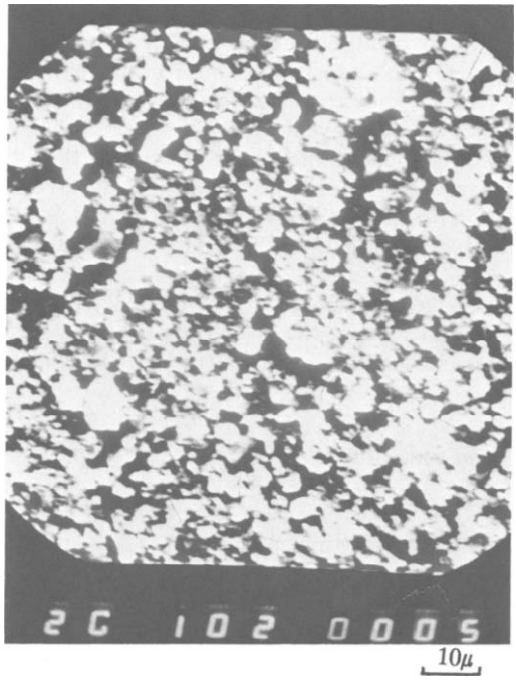

Fig. 1. Schematic of microbattery: (1) stainless-steel plate; (2) lithium film; (3) PAN-based electrolyte, and (4) $YBa_2Cu_3O_{7-\delta}$-cathode film.

Fig. 2. Surface microstructure of cathode film of battery B.

Results and discussion

Scanning electron microscopy (SEM) picture of a cathode film of battery B is shown in Fig. 2. Since the PAN-based electrolyte film is soft and exhibits high mechanical strength, both the contact between cathode and electrolyte, and the contact between electrolyte and Li is good.

Figures 3(a) and 3(b) show the impedance spectra of battery A and B, respectively. Figures 3(d) and 3(e) show the data plotted as real part and imaginary part against $\omega^{-1/2}$. This type of plot was introduced in a slightly simpler form by Randles [6]. Here, the relaxation in the real part is due to the double layer and the corresponding hump in the imaginary part should extend over several decades of frequency as observed. At lower frequencies, the curves become straight lines which are not quite parallel.

As a circuit, a battery may always be represented as an ideal voltage source (i.e., without any internal impedance) in series with a combination of a reactance

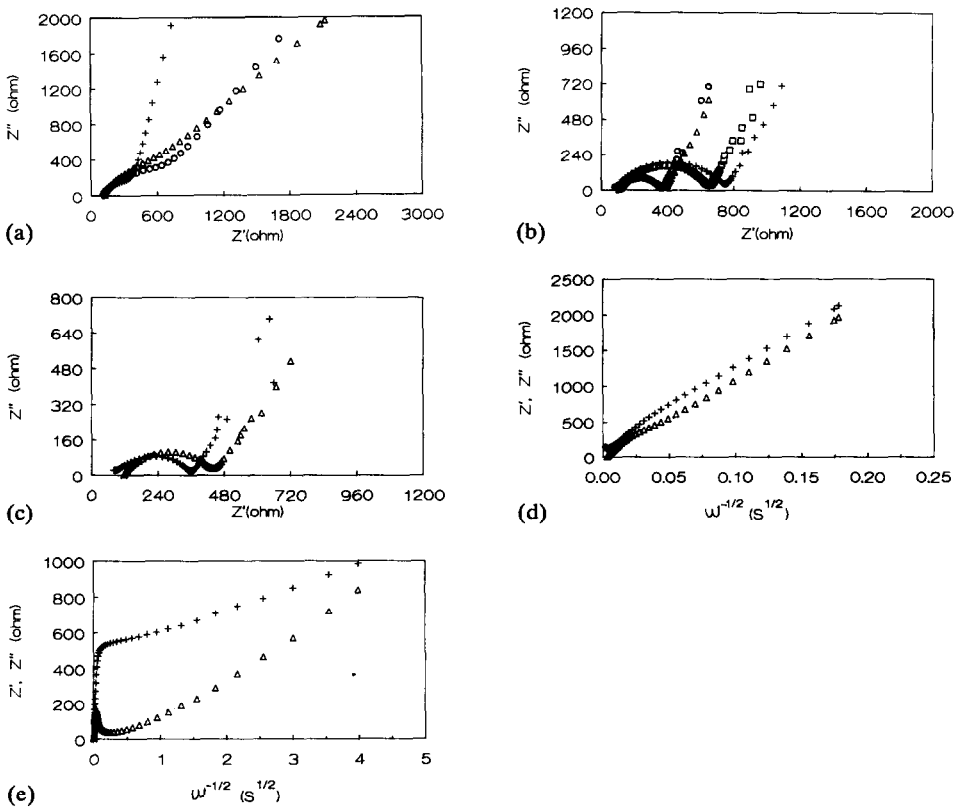

Fig. 3. (a) Impedance spectra of battery A: (+) new battery; (△) after first discharge, and (○) after 54 cycles. (b) Impedance spectra of battery B: (+) new battery; (△) after 33 cycles; (○) after 85 cycles, and (□) after 151 cycles. (c) Impedance spectra of battery B at different OCV after 85 cycles: (+) after 85 cycles and charged to OCV = 3.35 V (equilibrium), and (△) after 85 cycles and discharged to OCV = 2.02 V (equilibrium). (d) Frequency dependence of the real (R_s) and imaginary ($1/C_s$) part of the impedance of battery A: (+) real part, and 2 (△) imaginary part. (e) Frequency dependence of the real (R_s) and imaginary ($1/C_s$) part of the impedance of battery B: (+) real part, and (△) imaginary part.

(usually capacitive) and a resistance in either a parallel mode (R_p–C_p) or a series mode (R_s–C_s) [7].

The impedance of each electrode of a cell forms the double layer capacitance and leads inductance. The electrolyte solution will contribute a resistance to the battery impedance. Finally, the battery electrodes will contribute a 'geometrical' capacitance due to their close parallel spacing. Taking into account the above-mentioned facts, the equivalent circuit of a battery may be represented, as shown in Fig. 4(a). Taken into account that the inductive reactance and geometric capacitance are small compared with the measured capacitance by several orders, L_a, L_c and C_g have been omitted. Thus, a modified equivalent circuit of a cell can be used. The form of the complex plane plot suggests that the equivalent circuit of Fig. 4(b) would be a first approximation to the electrode analogue. Figure 5 shows the NNLS fit results compared with the experimental results of battery A and battery B.

Impedance spectroscopy (IS) of battery A and B shows that the resistance of the electrolyte and charge-transfer resistance are the same (see Table 1). The charge-transfer resistance is influenced by the deepness of the discharge as shown in Fig. 3(c). The Warburg impedance is represented by:

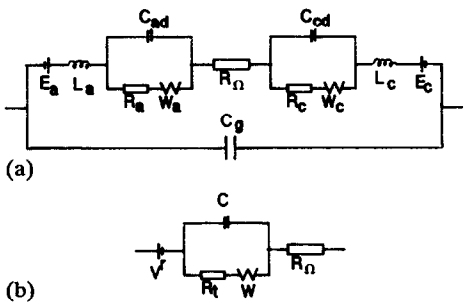

Fig. 4. (a) General equivalent circuit of a battery: E_a, E_c = single electrode potentials; L_a, L_c = lead inductances; C_{ad}, C_{cd} = double layer capacitance; R_a, R_c = charge-transfer resistances; W_a, W_c = Warburg impedances; R_Ω = resistance of electrolyte, and C_g = geometric capacitance. (b) Simplified equivalent circuit of a battery: $V' = E_c - E_a$ = emf of the battery; R_t = charge-transfer resistance; W = Warburg impedance; C_d = double-layer capacitance, and R_Ω = resistance of the electrolyte.

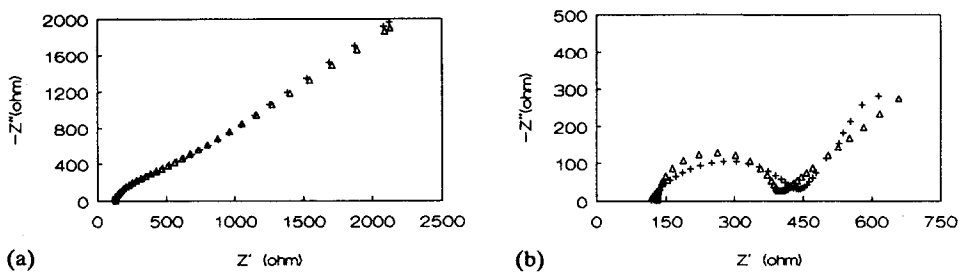

Fig. 5. (a) Non-linear least-square (NNLS) fit data comparing with the experimental impedance spectra of battery A after first discharge: (+) experimental, and (△) simulation. (b) NNLS fit data comparing with the experimental impedance spectra of battery B after first discharge: (+) experimental, and (△) simulation.

TABLE 1

Non-linear least-square (NNLS) fit results versus impedance spectra of battery A and B after first discharge

	Battery A	Battery B
R_Ω (Ω)	128.7	130.8
R_t (Ω)	244.8	253.4
Warburg, Yo (Ω^{-1})	6.673×10^{-5}	4.01×10^{-3}
Capacitance (F)	5.385×10^{-7}	1.271×10^{-6}

$$Z_W = K_W(i\omega)^{-1/2} \quad (1)$$

where, K_W is the Warburg coefficient. The value of the Warburg coefficient, K_W, can be obtained from the low-frequency slope of either real or imaginary part in the plot $\omega^{-1/2}$. The Warburg impedance was found to be the main reason for the high polarization losses of battery A. This is also apparent from the discharge curve in Fig. 5.

The negative electrode is metallic Li, and the electronic conductivity is more than sufficient for the current density to be expected in the battery.

The electronic conductivity of positive materials, $YBa_2Cu_3O_{7-\delta}$ is high, but the electronic conductivity of cathode film is lower by mixing with electrolyte to improve the ionic conductivity.

High Warburg coefficient is due to a low Li^+ diffusion coefficient. In battery A, Li^+ diffused slowly because little electrolyte permeated into the cathode film with a compact texture. In battery B, the cathode film became looser when carbon was added, a part of the electrolyte permeated into the cathode film, and the Warburg resistance decreased. The battery was found to discharge efficiently at considerably higher current densities. Figures 6(a) and 6(b) show the discharge curves of battery A and B under different current density, respectively. For the battery using cathode film A, the d.c. polarization lowered after 54 cycles. This phenomenon may be ascribed to the non-uniformity of the electrolyte layer and the interface-contact problem for a new battery. Figure 3(a) shows the impedance spectra of the new battery after first discharge, and after 54 cycles. It is observed that the Warburg impedance of the new battery is high, and most probably caused by slow diffusion through the interface layer.

Figure 6(c) shows the discharge curve of battery B at 40 $\mu A/cm^2$. The d.c. polarization increases slowly with the number of cycles. Compared with the impedance spectra, we find that the Warburg resistance increases slowly with the number of cycles. The electrolyte resistance (R_Ω) is almost constant. The difference in charge-transfer resistance (R_t) may be ascribed to the different charge state of the battery. Figure 3(c) shows impedance spectra of battery B with different open-circuit voltage after 85 cycles. R_t increases with the depth-of-discharge.

Conclusions

A microbattery comprising a ceramic superconductor $YBa_2Cu_3O_{7-\delta}$ cathode, and PAN-based polymer electrolyte exhibits high discharge efficiency at high current density and has a good cyclic behaviour. In general, the added carbon improves the electronic conductivity of the cathode film and reduces the charge-transfer resistance. In this

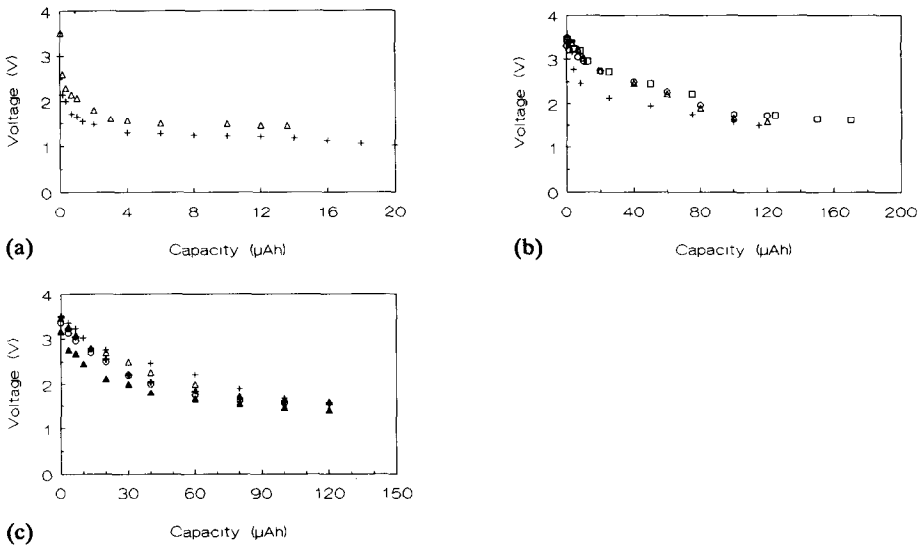

Fig. 6. (a) Discharge curve of battery A on first and after 54 cycles at 4 $\mu A/cm^2$: (+) first discharge, and (△) after 54 cycles. (b) discharge curve of battery B at different current densities: (+) 100 $\mu m/cm^2$; (△) 40 $\mu m/cm^2$; (○) 20 $\mu m/cm^2$, and (□) 10 $\mu m/cm^2$. (c) Discharge curve of battery B at 40 $\mu A/cm^2$ under different cycles: (+) 4; (△) 34; (○) 85; (+) 152, and (▲) 202 cycles.

experiment, it is found that the diffusion process has been improved and the Warburg resistance has been reduced by the added carbon.

References

1 M. B. Armand, J. M. Chabagno and M. J. Duclot, in P. Vashista, J. N. Mundy and G. K. Shenoy (eds.), *Fast Ion Transport in Solids,* Elsevier, Amsterdam, 1979, p. 131.
2 L. Q. Chen, A. van Zomeren and J. Schoonman, *Solid State Ionics, 50* (1992) 55.
3 K. M. Abraham and M. Alamgir, *J. Electrochem. Soc., 137* (1990) 1657.
4 H. Huang, L. Q. Chen, X. J. Huang and R. J. Xue, *Ext. Abstr., 3rd Int. Symp. Polymer Electrolytes, Annecy, France, June 17–21, 1991,* p. 111, *Electrochim. Acta,* to be published.
5 Z. X. Zhong, L. Q. Chen, Q. S. Yang, Y. Z. Huang, G. H. Chen, R. M. Wang, G. R. Liu, C. G. Cui and L. Chen, *KeXue Tongbao, 321* (1987) 661.
6 J. E. B. Randles, *Discuss. Faraday Soc., 1* (1947) 11.
7 S. Sathyanarayana, S. Venugopalan and M. L. Gopikanth, *J. Appl. Electrochem., 9* (1979) 125.